In Situ Localization of Lettuce Infectious Yellows and Maize Stripe Viruses by Immunogold Labeling and Laser Scanning Confocal Microscopy in Refected Signal Detection Mode

*G.[1], Rodrigo; J.[2], Wierzchos; T.[3], Tlan; B.W.[3], Falk; V.[1] *, Medina.*
[1] Dept. de Producció Vegetal i Ciència Forestal. Universitat de Lleida. (UdL). Avda. Alcalde Rovira Roure, 177. 25198 Lleida, Spain. [2] SUIC-ME. UdL., Avda. Alcalde Rovira Roure 44, 25006 Lleida, Spain. [3] Dept. of Plant Pathology, University of California , 1 Shields Avenue, Davis, CA 95616, USA.
(*) Author for correspondance (Fax: 34-973-238264). E-mail: medinap@pvcf.udl.es

Abstract

Colloidal gold is a very extensively used label for light and electron microscopy and its advantages opposite fluorochromes are well known. However, it is difficult to resolve by optical microscopy without silver enhancement procedures. The techniques described herein provide for the detection of immunogold labeled plant viruses using laser scanning confocal microscopy in reflected signal detection mode. Antibody-conjugated colloidal gold particles observed by reflected laser light signals were localized in either tissues of lettuce infectious yellows (LIYV) and maize stripe viruses-infected plant samples or LIYV-infected protoplasts and coincided with immunolabeled areas observed by transmission and scanning electron microscopy. The technique permits visualization of gold labeling avoiding silver enhancement on semithin sections and resin blocks; however, in some cases, other reflected light signals can interfere. This technique could be useful as a complement to, or alternative for immuno-electron microscopic studies.

KEYWORDS: IGL, LSCM, Plant Viruses, Reflected Signal Detection Mode. SEM-BSE, TEM.

Introduction

The advantages of colloidal gold opposite fluorochromes are numerous in immunohistochemical studies: a) it is more stable; b) it sends out stronger and more permanent signals; c) it has a greater penetration capacity into sections, providing three dimensional reconstruction possibilities; d) it increases the possibilities for multiple labeling studies; e) it does not produce fluorescence bleaching, a principal fluorochrome limitation, and f) the possible autofluorescence of tissue does not interfere with the labeled image (7, 14, 15, 18, 19). However the tiny size of gold particles makes their resolution by optical wavelengths very difficult, and it is usually necessary to improve the labeling by silver enhancement. Irregardless, based on its technical advantages and better sensitivity and performance, some authors assume that colloidal gold labeling with silver enhancement is even better than other alternatives as immunofluorescence for light microscopy (22, 25).

Several fluorochromes are widely used with good results in plant immunochemical and/or histochemical studies (4,16, 20, 21). However, strong autofluorescence of some plant tissues can be a problem using some fluorochromes. In these cases colloidal gold labeling alone and/or with some kind of enhancement could be an alternative technique. The colloidal gold particles are able to scatter photons in characteristic ways and it is possible to localize them using conventional microscopy, dark-field or confocal microscopy by capturing the light reflected by the gold particles (6). Colloidal gold imaging in the reflectance mode has begun to replace fluorochromes for non-isotopic detection systems, for example, for *in situ* hybridization techniques (14, 15).

Laser scanning confocal microscopy (LSCM) is a technique that allows obtaining high resolution and high contrast information from single confocal sections. Because of the advantages of confocal microscopy, we have tested the possibility for detection of antibody-conjugated colloidal gold particles used for immunogold labeling (IGL), by using laser scanning confocal microscopy (LSCM) in the reflectance signal detection mode. Comparison of the proposed LSCM method with a standard fluorochrome labeling was also performed in order to localize plant viruses in resin embedded infected plant samples. The IGL was carried out either on resin blocks and sections from them, of embedded plant virus-infected tissues. We used two viral infection models that we have studied extensively for several years: Lettuce infectious yellows crinivirus (LIYV) infecting specifically phloem cells (8, 9), and Maize stripe tenuivirus

(MStV) which induces the formation of abundant amorphous semi-electron-opaque inclusions bodies (ASO) visible in mesophyll cells (1,11). In the LIYV case we also tested the technique on RNA1-inoculated protoplasts not-expressing the coat protein (CP) of LIYV, and RNA1+RNA2-inoculated protoplasts, expressing LIYV-CP (13, 17). The use of this technique as a previous step before immuno-electronmicroscopy procedures is discussed.

Materials and Methods

Plant material, protoplasts and antisera

Healthy and infected leaves of lettuce (*Lactuca sativa* L., cv. Summer Bibb) and tobacco (*Nicotiana benthamiana* Domin) plants, mock-inoculated and LIYV-RNA-inoculated (RNA 1 or RNA1+RNA2) tobacco mesophyll protoplasts (17), together a specific polyclonal antiserum against the LIYV capsid protein (LIYV-CP-As) (13) were used to localize LIYV antigens. The plant tissue (small pieces 1x10 mm of leaf), and protoplasts collected by low speed centrifugation, were embedded at low temperature in LR White, medium grade (London Resin White, Hants, UK) according to Wells' protocol (26). For analysis of MStV, healthy and infected leaves of maize (*Zea mays* L.), processed as above, and using a specific polyclonal antiserum against MStV non-capsid protein (MStV-NCP-As) which specifically labels ASO inclusion bodies (10) were used.

Immunolabeling and confocal microscopy

Semithin sections (2-2,5 µm) of embedded samples (blocks) were obtained using an ultramicrotome (Reichert, Ultracut). Every section was deposited on a distilled water drop on a gelatinized slide, and dried at room temperature. Because the sectioned side of the blocks were to be treated as well, the opposite side was stuck on a slide to facilitate the subsequent manipulation and posterior observation.

The incubation was conducted as follows: 1) one hour in blocking buffer (10 mM Tris-HCl, pH: 7,4; 150 mM NaCl; 1%BSA; 0,05% Tween 20) at room temperature, 2) three hours with specific antisera diluted in blocking buffer (1:100) at room temperature, 3) 0,5 hour with blocking buffer at room temperature, 4) one hour with a secondary antiserum, 30nm gold conjugated IgG goat anti-rabbit (BBInternational, Cardiff, UK) or rhodamine conjugated $F(ab)'_2$ anti-rabbit (Boehringer, Mannheim GmbH, Germany) diluted in blocking buffer (1:20) at room temperature. Distilled water washings were done at every change.

The slides containing sections were mounted with cover slips and Fluoromount-G (Electron Microscopy Sciences, USA). The blocks were observed directly with 60x/1.4 NA oil-immersion objective lens.

LSCM (LSM 310 - Zeiss) observations were performed employing different lasers and filter combinations. Reflected light (RL) from colloidal gold labeling was detected using He/Ne laser ($\lambda = 543$nm) without any filter following Cogswell *et al.* (5). Fluorescence of rhodamine labeling (FL) was observed with the same laser but using a BP filter ($575 < \lambda < 640$nm) following the supplier instructions. Samples were also analyzed using transmitted light (TL) and the same microscope. To detect the autofluorescence signals (AF), samples were excited by an Ar laser ($\lambda = 488$nm) and the signal was detected using a LP filter ($\lambda > 543$nm). All LCSM images proceeded from single confocal optical sections.

Immuno-electronmicroscopy

In order to confirm and verify the efficacy of LSCM for detection of immunogold labeled particles, serial ultrathin sections obtained from the same blocks were immunogold labeled using 10nm gold. After standard contrasting (uranyl acetate) and staining (lead citrate) the ultrathin sections were observed using transmission electron microscopy (TEM; EM 910, Zeiss). Moreover, the block surfaces containing biological material were also immunogold labeled with 30nm gold particles. After coating with evaporated carbon the block surfaces were observed using scanning electron microscopy operated in back-scattered electron (SEM-BSE) detection mode. The BSE detector records discriminatory differences in atomic number of the target, and features composed of heavier elements such as gold particles, will appear brighter than will those of lighter composition, such as the organic matrix. This SEM-BSE detection of immunogold particles were performed after Ascaso *et al.* (2) and Ascaso *et al.* (3) using DSM 942A (Zeiss) equipped with BSE solid state detector.

Results

Confocal microscopy in reflectance signal detection mode

LIYV-infected lettuce and tobacco tissues showed RL signals in phloem cells (Figs. 1B, 1F and 2B). These were not observed in healthy samples (Figs. 1D, 1H and 2D). Intense RL signals were also sometimes detected in non-phloem tissues of both healthy and infected specimens and either sections (Figs. 1B, 1D, 1F and 1H) or blocks (Figs. 2B and 2D). However, most of these intense RL signals coincided with wrinkles, crumples, stripes and others defects present in these specimens as can be identified from observation of the TL images.

Protoplasts inoculated with LIYV-RNA1+2 showed RL signals in cytoplasm (Fig. 3B). These signals were not detected from neither LIYV-RNA1-inoculated protoplasts (Fig. 3D) nor mock-inoculated (not showed), although intense RL

signals related with defects of sections were observed in all specimens.

RL signals were localized in mesophyll and parenchyma cells containing ASO inclusion bodies for MStV-infected maize samples (Fig. 4B). The ASO inclusion bodies can be visualized in TL images (Fig. 4A). Healthy samples did not show similar RL signals (Fig. 4D). However, in both cases, intense signals were seen for both healthy and infected tissues but were associated with different observable defects as can be seen in TL images. Infected samples (sections or blocks) without IGL were also observed to determine if ASO inclusion bodies alone could produce RL signals. These observations did not show RL signals from ASO bodies.

Confocal immunofluorescence

There were no detectable differences between the fluorescence labeling of healthy and infected tissues using rhodamine. It was not possible to distinguish these tissues even when subtracting part of the natural autofluorescence, or though modifying contrast and brightness parameters.

Immuno-electronmicroscopy

IGL of ultrathin sections allowed us to confirm the source of the RL signals observed by LSCM. LIYV infected plant tissue showed the cytoplasm of phloem cells to be specifically labeled (Fig. 5). A low level of labeling was localized on chloroplasts of LIYV-infected tobacco tissue and non-specific labeling of tracheids was observed in both healthy and LIYV-infected tissue of lettuce and tobacco (not shown). IGL was localized in the cytoplasm containing filamentous particles of LIYV-RNA1+2-inoculated protoplasts only (see 17).

Labeling was specifically localized to mesophyll and parenchyma cells containing ASO inclusions of MStV-infected samples (Fig. 6). Neither infected tissue without ASO nor healthy maize showed detectable IGL.

LIYV-infected samples showed BSE signals in phloem cells and, in the case of infected tobacco samples, were also observed in chloroplast (not shown). ASO inclusion bodies of MStV-infected samples showed BSE signals (Figs. 7A and B). Healthy maize did not show these signals (Fig. 7C).

Discussion

To use LSCM in reflectance, Cogswell *et al.* (5); Cogswell (6) and Linares-Cruz *et al.* (15) advise to compare very carefully infected samples with healthy controls to distinguish authentic IGL-RL signals from others. According to Cogswell *et al.* (5) this comparison is difficult because some organelles, cellular structures and other cellular particles produce RL signals when plant tissues are examined with different wavelengths, due to the Rayleigh scattering phenomenon. Perhaps this phenomenon is interfering in some of the images obtained in our study. Virus-infected plant cells exhibit many changes due to viral infection including crystals, disruption of organelles, and other alterations, all of which can produce RL even in the absence of IGL. These can be difficult to distinguish from reflectance due to the presence of gold particles and IGL. Obviously the level of discrimination/resolution of this technique is closely related with the abundance of labeling, as occurs with many other used labeling techniques.

Furthermore, additional distortion and reflectance can result from defects and imperfections in tissues resulting from specimen manipulation. However in this case the superposition of RL and TL signals helps to readily distinguish and identify RL resulting from gold particles associated with IGL. Therefore, it is very important to avoid wrinkles, crumples and holes in semithin sections, and impurities of resin of blocks in order to get clear images.

LSCM can generate clear thin optical section images totally free from out-of-focus signals thereby permitting localization of RL signals and reproduction of plant tissue (TL signals) without additional manipulation, as reported Inoué (12). However, when using whole blocks, the required optical sectioning incorporates scattered photons resulting from the defects present in the resin and the rest of the specimen (Fig. 2).

Rhodamine is employed in many immunolabeling studies of plants and AF and FL signals to identify its location within cells (16). In our case, we were not able to differentiate between AF and FL of rhodamine labeling in maize, lettuce and tobacco samples. This is because the FL signals are really composed of AF and FL rhodamine signals, as has been shown by McCormac *et al.* (16), and it is very difficult to separate them with the filters used. When rhodamine labeling is observed, intense AF signals are gathered and are sometimes more intense than those due to rhodamine. These authors state that some LSCM parameter modifications allow detection of less intense AF signals in order to more easily identify fluorochrome labeling. However, the plant AF spectrum includes rhodamine and thus it can not be separated. So, according to Slavik (23) the basic requirement to use fluorochromes is not followed, because it is necessary that both AF and fluorochrome signals be distinguished. A possible solution that would allow localization of rhodamine labeling would be to eliminate plant AF through chemical (23) or dye treatments (24) or perhaps by using other filters. However, these alternatives have not been followed. Alternatively, the use of other fluorochromes could avoid these problems, but this was not the objective of our study.

One limitation of the use of LSCM observations is that it allows detecting different kinds of signals, but these received signals are constrained. Microscope parameters can be used

to detect low intensity signals, but by changing these parameters it is also possible to obtain high quality images, for example, by modification of the pinhole aperture. By this, gold particles would have their strongest scattering peak in the green portion of the spectrum (550 nm) (6), but the images would not show the actual intensity observed because other smaller particles present in the specimen could scatter at the same portion of spectrum. Thus, when intensity is increased, it is not possible to determine which are the real IGL-RL signals. It is not often possible to reproduce observations with the same parameters because LSCM automatic parameters fix later observation conditions and every sample has different characteristics.

This work shows that LSCM in reflectance mode allows detecting viruses and IGL specifically in plants or protoplasts. It was observed that plant autofluorescence does not interfere with reflected light signal generated by colloidal gold. It also was shown that the visualized RL signals were localized in the same regions observed with TEM and SEM-BSE techniques. This light microscopy technique detects the reflected light from the gold particles. Obviously the signals from gold could be amplified by silver enhancement but they are sufficiently clear without further enhancement. This technique as described or enhanced with silver could be very useful as a complement and/or alternative to TEM or SEM-BSE observations. In the case of tissues with a complex organization and structure, LSCM techniques would allow a preliminary labeling location and facilitate identification of sites to be chosen for TEM observation. Detection of specific immunogold-labeled regions on biological materials such as block surfaces could significantly facilitate efficient subsequent ultrathin sectioning to only areas of interest for TEM examination. Our future studies based on LSCM detection of immunogold colloidal particles will involve attempts to localize viruses in their insect vectors. The LSCM technique described herein could greatly facilitate IGL localization of plant viruses within the complex internal anatomy of insects vectors.

References

1. Ammar, E.D., Gingery, R.E., Nault, L.R. (1985) Two types of inclusions in maize infected with maize stripe virus. Phytopathology, 75:84-89.

2. Ascaso, C., Wierzchos, J., de los Rios, A. (1995) Cytological investigations of lithobiontic microorganisms in granitic rocks. Botanica Acta, 108:474-481.

3. Ascaso, C., Wierzchos, J., de los Rios, A. (1998) *In situ* investigations of lichens invading rock at cellular and enzymatic level. Symbiosis, 24:221-234.

4. Baulcome, D.C., Chapman, S., Santa-Cruz, S. (1995) Jellyfish green fluorescent protein as reported for virus infections. Plant Journal, 7:1045-1053.

5. Cogswell, C.J., Hamilton, D.K., Sheppard, C.J.R. (1992) Colour confocal reflection microscopy using red, green and blue lasers. Journal of Microscopy, 165: 103-117.

6. Cogswell, C.J. (1995) Imaging immunogold labels with confocal microscopy (ed. J. Pawley) Plenum Press. pp: 507-513.

7. Cornelese-Ten Velde, I., Prins, F.A. (1990) New sensitive light microscopical detection of colloidal gold on ultrathin sections by RCM. Histochemistry, 94:61-71.

8. Duffus, J.E., Larsen, R.C., Liu, H.Y. (1986) Lettuce infectious yellows virus a new type of whitefly-transmitted viruses. Phytopatology, 76:97-101.

9. Duffus, J.E., Mayhew, D.E., Flock, R.A. (1982) Lettuce infectious yellows a new type of whitefly-transmitted virus of the desert southwest. Phytopathology, 72:963.

10. Espinoza, A.M., Pereira, R., Macaya-Lizano, A.V., Hernández, M., Goulden, M., Rivera, C. (1993). Comparative light and electron microscopic analyses of tenuivirus major noncapsid protein (NCP) inclusion bodies in infected plants, and of the NCP *in vitro*. Virology, 195:156-166.

11. Gingery, R.E., Nault, L.R., Bradfute, O.E. (1988) Maize stripe virus: characteristics of a member of a new virus class. Virology, 112:99-108.

12. Inoué, S. (1995) Foundations of confocal scanned imaging in light microscopy (ed J. Pawley) Plenum Press. pp: 1-17.

13. Klaassen, V.A., Boeshore, M., Dolja, V., Falk, B.W. (1994) Partial characterization of the Lettuce infectious yellows virus genomic RNAs, identification of the coat protein gene, and comparison of its aminoacid sequence with other filamentous RNA plant viruses. Journal of General Virology, 75:1525-1533.

14. Linares-Cruz, G., Chassoux, D., Millot, G., Schmid, M., Calvo, F. (1995) Aplicación combinada de la microscopía confocal en fluorescencia y reflectancia en células y tejidos humanos (ed A. Sampedro, J.R. de los Toyos, A. Martínez-Nistal) Servicio de publicaciones de la Universidad de Oviedo. pp: 85-97.

15. Linares-Cruz, G., Rigaut, J.P., Vassy, J., de Oliveira, T.C., de Cremoux, P., Olofsson, B., Calvo, F. (1994) Reflectance *in situ* hybridization (RISH): detection by confocal reflectance laser microscopy, of gold labeled riboprobes in breast cancer cell lines and histological specimens. Journal of Microscopy, 173:27-38.

16. McCormac, D., Boinski, J.J., Ramsperger, V.X., Berry, J.O. (1997) C_4 gene expression in photosynthetic and non-photosynthetic leaf regions of *Amaranthus tricolor*. Plant Physiology, 114:801-815.

17. Medina, V., Tian, T., Wierzchos, J., Falk, B.W. (1998) Specific inclusion bodies are associated with replication of Lettuce infectious yellows virus RNAs in *Nicotiana benthamiana* protoplasts. Journal of General Virology, 79:2325-2329.

18. Paddock, S., Mahoney, S., Minshall, M., Smith, L., Duvic, M., Lewis, D. (1991) Improved detection of *in situ* hybridization by laser scanning confocal microscopy. Biotechniques, 2:486-493.

19. Rigaut, J.P., Linares-Cruz, G., Vassy, J., Downs, A.M., de Oliveira, T.C., de Cremoux, P., Calvo, F. (1993) Reflectance *in situ* hybridization (RISH)-3-D confocal laser imaging and quantitation after immunogold labelling of a riboprobe. Cytometry, 6:22 (supl.)

20. Roberts, A.G., Santa-Cruz, S., Roberts, I.A., Prior, D.A.M., Turgeon, R., Oparka, K.J. (1997) Phloem unloading in sink leaves of *Nicotiana benthamiana*: comparison of a fluorescent solute with a fluorescent virus. The Plant Cell, 9:1381-1396.

21. Santa-Cruz, S., Chapman, S., Roberts, A.G., Prior, D.A.M. (1996) Assembly and movement of a plant virus carring a green fluorescent protein overcoat. Proc-Natl-Acad-Sci-USA, 93:6286-6290.

22. Scopsi, L. (1989) Silver-enhanced colloidal gold method (ed M.A. Hayat) Academic Press. pp: 251-296.

23. Slavik, J. (1994) Fluorescent dyes and cells (ed. J. Slavik) CRC Press. pp: 13-35.

24. Thonat, C., Mathieu, C., Crevecoeur, M., Penel, C., Gaspar, T., Boyer, N. (1997) Effects of a mechanical stimulation on localization of annexin-like proteins in *Bryonia dioica*. Plant Physiology, 114:981-988.

25. Vandenbosch, K.A. (1991) Immunogold labeling (ed J.L. Hall, C. Hawes) Academic Press. pp: 181-218.

26. Wells, B. (1985) Low temperature box and tissue handling device for embedding biological tissue for immunostaining in electron microscopy. Micron and Microscopica Acta 16, 763-767.

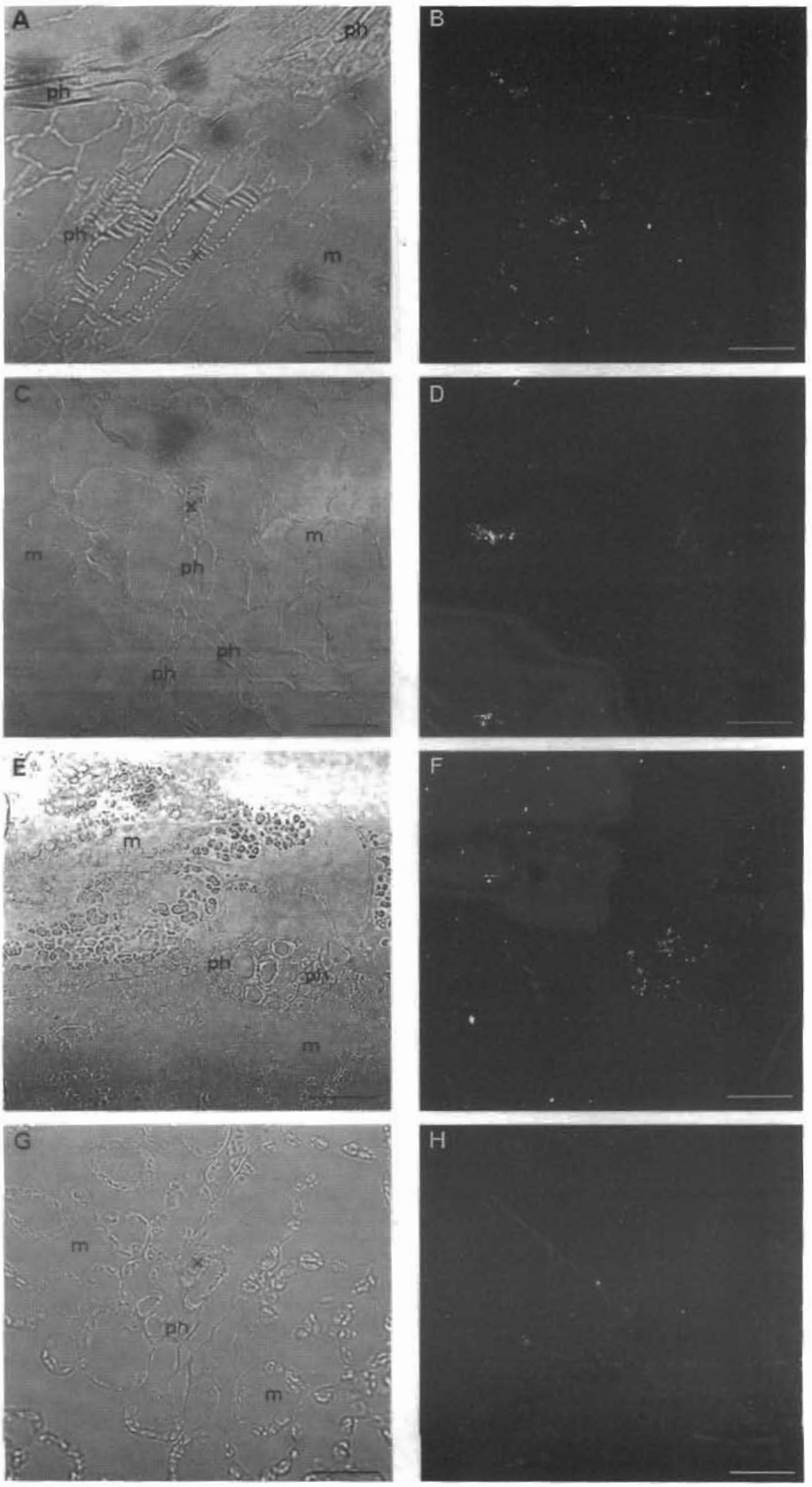

Figure 1. LSCM images of immunogold labeled semithin sections of lettuce infectious yellows crinivirus (LIYV)-infected (A-B, E-F) and healthy (C-D, G-H) lettuce (A-D) and tobacco (E-H) leaves. Left: transmitted light images. Right: corresponding reflected light signals images; (m: mesophyll; ph: phloem; x: xylem. Bar: 32.90 µm instead of m in all the figures; gold particle size: 30 nm).

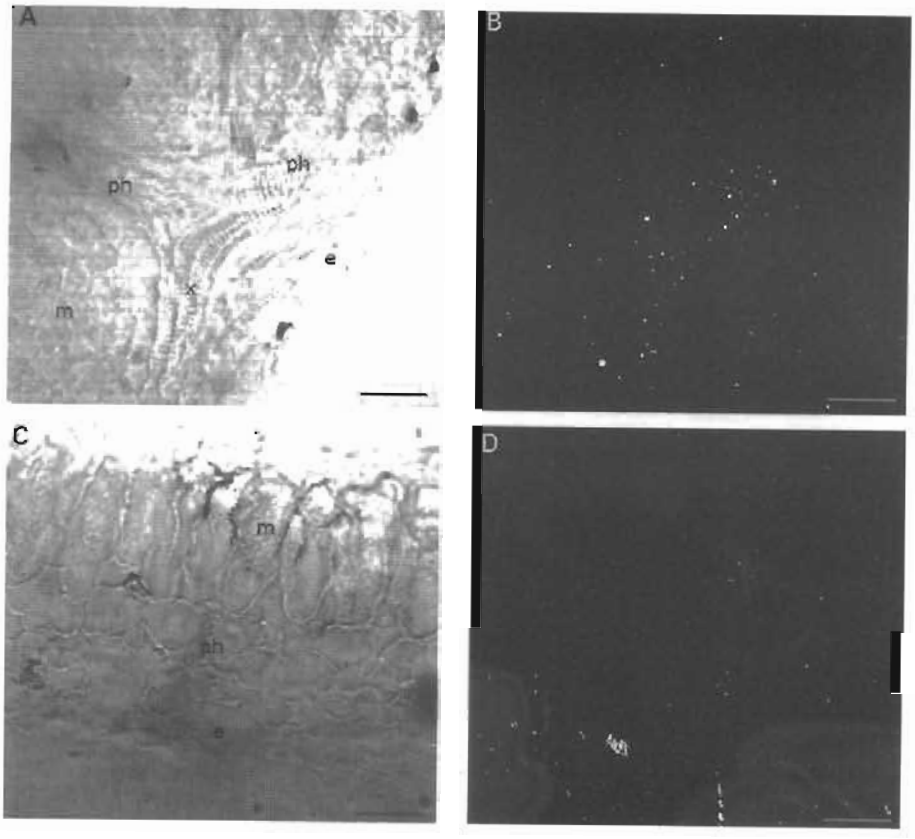

Figure 2. LSCM images of immunogold labeled resin blocks of lettuce infectious yellows crinivirus (LIYV)-infected (A-B) and healthy (C-D) lettuce leaves. Left: transmitted light images. Right: corresponding reflected light signals images; (e: epidermis; m: mesophyll; ph. phloem; x: xylem. Bar: 32,10 µm, gold particle size: 30 nm).

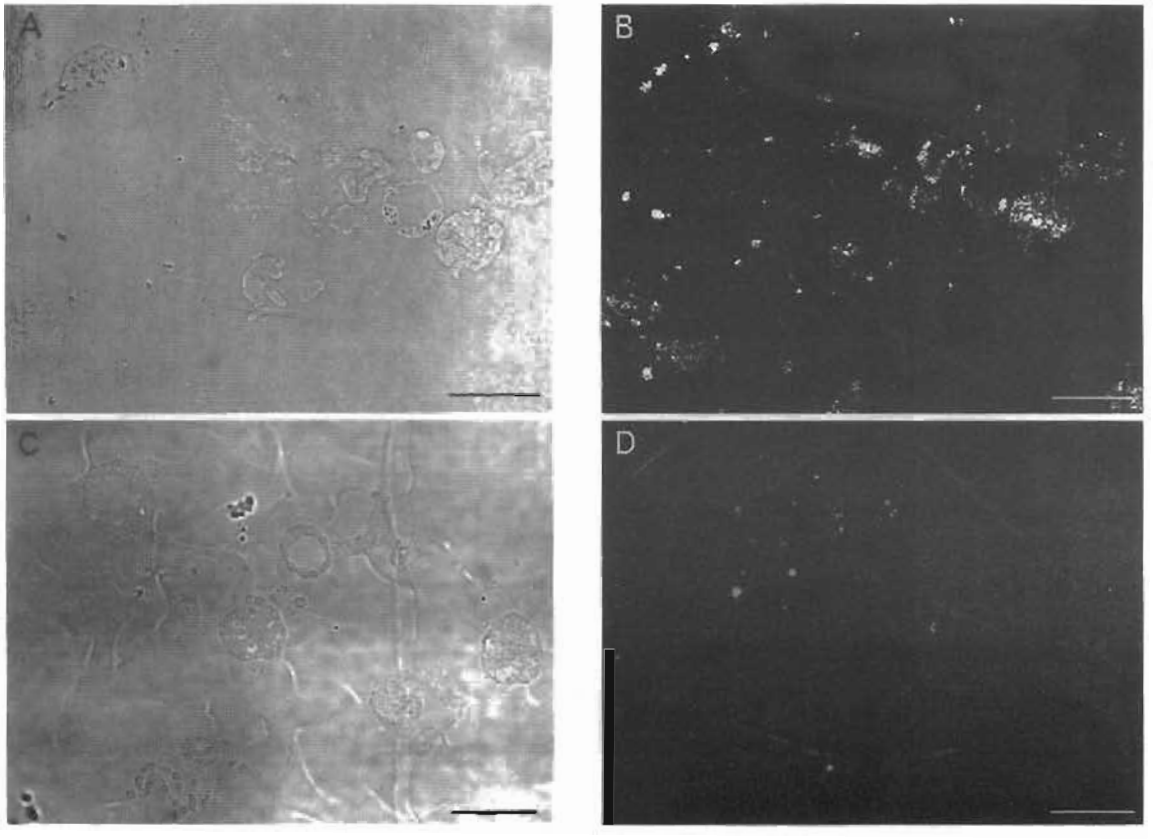

Figure 3. LSCM images of immunogold labeled semithin sections of lettuce infectious yellows crinivirus (LIYV)-inoculated protoplasts, LIYV-RNA1+2 (A-B) and LIYV-RNA1 (C-D). Left: transmitted light images. Right: corresponding reflected light signals images; (Bar : 32 µm; gold particle size: 30 nm).

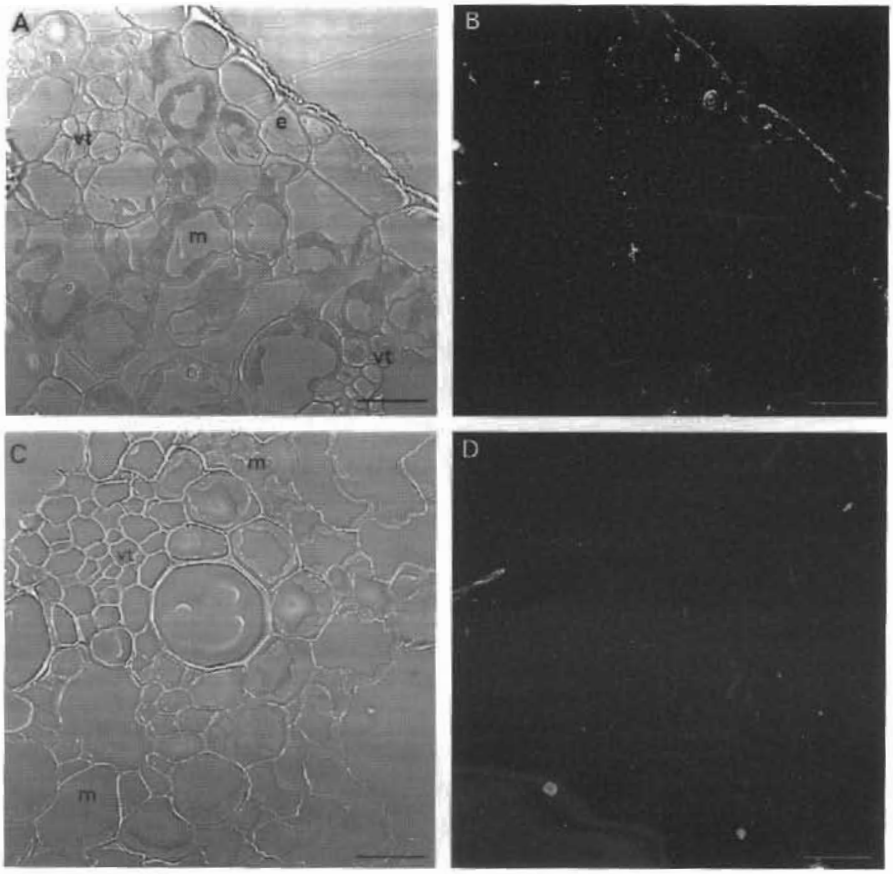

Figure 4. LSCM images of immunogold labeled semithin sections of infected (A-B) and healthy (C-D) maize leaves. Left: transmitted light images. Right: corresponding reflected light signals images; (e: epidermis; m: mesophyll; vt: vascular tissue. Bar: 23 µm; gold particle size: 30 nm).

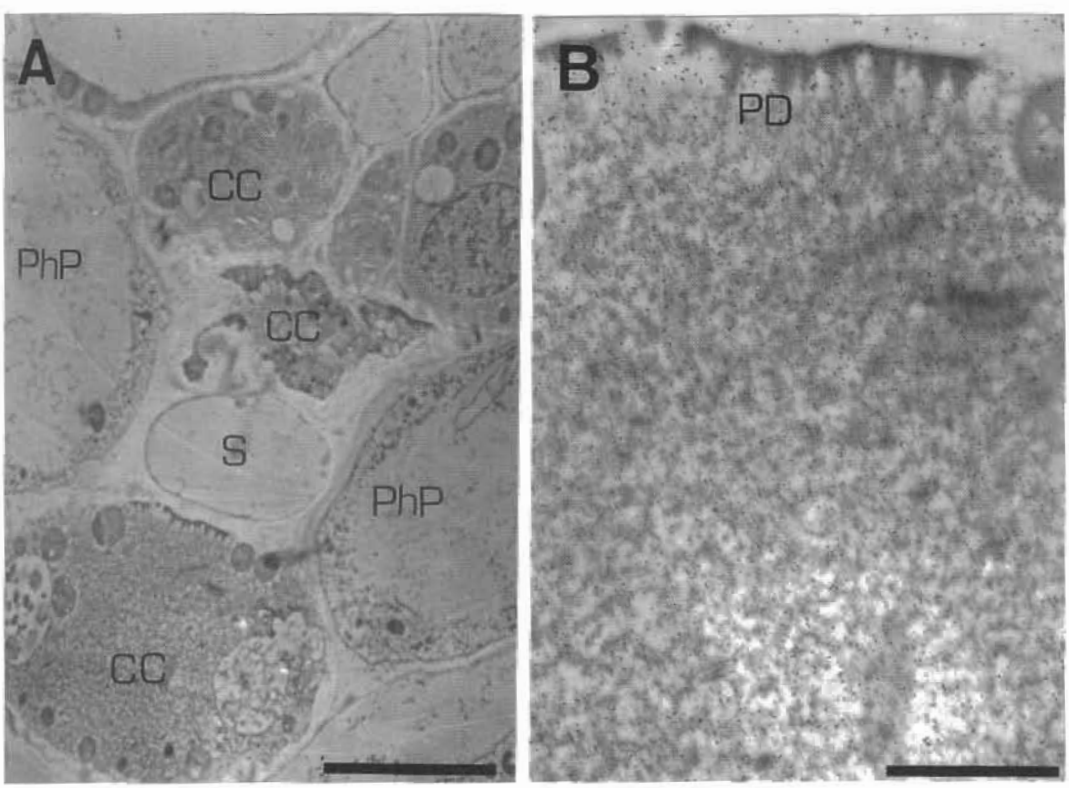

Figure 5. TEM images of immunogold labeled ultrathin sections of lettuce infectious yellows crinivirus-infected lettuce (A.) Lettuce phloem cells. (B) Detail of the lower cell of fig. A. Infected companion cell showing plasmalemma deposits and immunogold labeled cytoplasm. (CC: companion cell; PD: plasmalemma deposits; PhP: phloem parenchyma cell; S: sieve element. Bars: A=3,63 µm; B=0,91 µm; gold particle size: 10 nm).

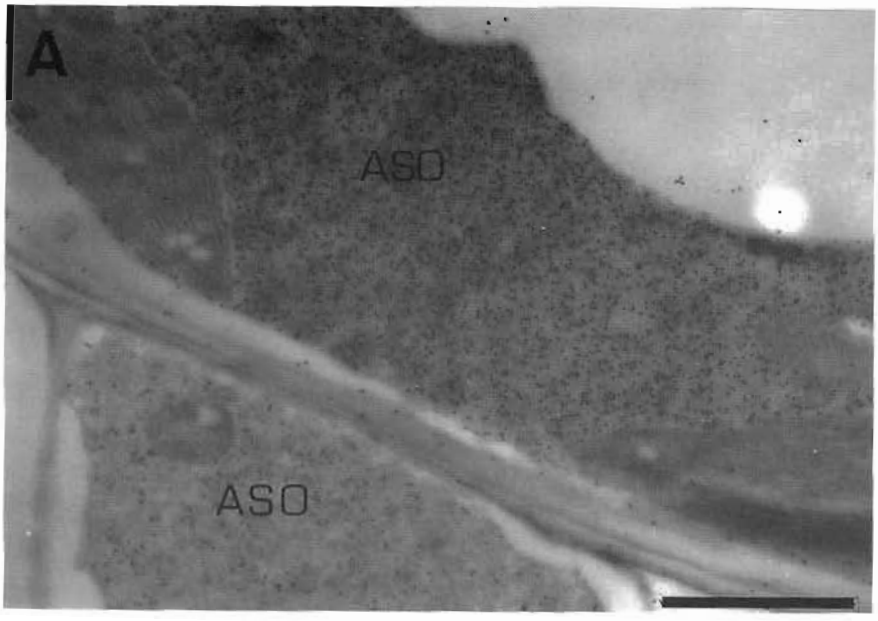

Figure 6. TEM image of immunogold labeled ultrathin section of maize stripe tenuivirus (MStV)-maize infected leave. Cell showing specific immunogold labeling of amorphous semi-electron opaque (ASC) inclusion bodies. (Bar. 1.1 µm; gold particle size. 10 nm).

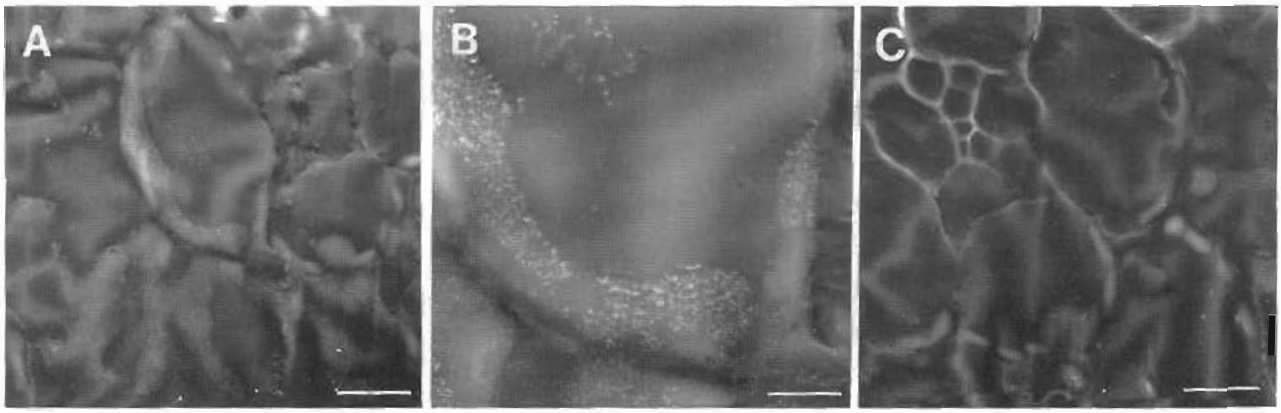

Figure 7. SEM-BSE images of immunogold labeled surfaces of resin blocks of maize stripe tenuivirus (MStV)-infected (A-B) and healthy (C) maize leaves. Immunogold labeling in amorphous semi-electron opaque (ASO) inclusion (A and B); (Bars: A=10 µm; B=5 m. gold particle size: 30 nm).